Modeling Finite-size effects in LES/DNS of Two-Phase Flows

Apte, S.V.[1], Mahesh, K.[2], and Lundgren, T.[2]

[1] Stanford University, Stanford, CA 94305 sapte@stanford.edu,
[2] University of Minnesota, Minneapolis, MN 55311 mahesh@aem.umn.edu, lundgren@aem.umn.edu

1 Introduction

Recent direct numerical simulation (DNS) of large number of solid particles interacting through a fluid medium by Joseph and collaborators [1, 2] show that a layer of heavy particles with fluid streaming above it can develop Kelvin-Helmholtz (K-H) instability waves whereas a layer of particles above a lighter fluid develops Rayleigh-Taylor instability. However, performing full DNS of millions of dispersed particles in a turbulent flow (e.g. spray combustion, liquid atomization, spray coating, fluidized bed combustion, aerosol transport) is computationally intensive. For such applications, the particle size is typically smaller than the grid-resolution used for the computation of the continuum fluid. Under these conditions, the particles are *subgrid* and some sort of subgrid modeling is necessary to simulate their motion.

The "point-particle" assumption is commonly employed where forces on the dispersed phase are computed through model coefficients. The effect of the particles on the carrier phase is represented by a force applied at the *centroid* of the particle. For dilute particle loadings with swirling, separated flows in a coaxial combustor computed using LES of point-particles, Apte *et al.* [3] indicated good agreement with the experimental data. However, for moderate loadings and wall-bounded flows, Segura *et al.* [4] have shown that the point-particle approximation fails to predict the turbulence modulation compared to experimental values. In order to capture the same level of turbulence modulation observed in experiments, it was required to artificially increase the particle loadings by an order of magnitude when using the point-particle approach [4]. In addition, if the particle size is greater than Kolmogorov scale, simple drag/lift laws used in this approach do not capture the unsteady wake effects [5, 6].

In this work we attempt to extend the point-particle approximation by accounting for the finite-size of the particles and the corresponding volume displacement (Θ_f) of the carrier phase. Accordingly, the carrier phase continuity and momentum equations are modified to include Θ_f. The formulation

was originally put forth by Dukowicz [7] in the context of spray simulations. However, the particle volume fractions are often neglected owing to the increased complexity of the governing equations as well as numerical stiffness they impose in the dense spray regime. Several studies on dense granular flows [8, 9, 10] use this model for laminar flows. Similar formulation has been applied for bubbly flows at low bubble concentrations to investigate the effect of bubbles on drag reduction in turbulent flows [11]. However, these studies do not identify the effects of the fluid displacement by dispersed phase compared to the point-particles. In the following sections, the mathematical model and numerical scheme are described in brief. The model is applied to simulate gravitational settling and fluidization by jet to validate the numerical scheme. Next we compute plane Poisuille flow with rigid spheres at the bottom to show particle dispersal and lift.

2 Mathematical Formulation

The formulation described below consists of the Eulerian fluid and Lagrangian particle equations, and accounts for the displacement of the fluid by the particles as well as the momentum exchange between them [12].

2.1 Gas-Phase Equations

The fluid mass for unit volume satisfies a continuity equation,

$$\frac{\partial}{\partial t}\left(\rho_f \Theta_f\right) + \bigtriangledown \cdot \left(\rho_f \Theta_f \mathbf{u}_f\right) = 0 \tag{1}$$

where ρ_f, Θ_f, and $\mathbf{u}_f$ are the fluid density, volume fraction, and velocity, respectively. This indicates that the average velocity field of the fluid phase does not satisfy the divergence-free condition even if we consider an incompressible suspending fluid. The particle volume fraction, $\Theta_p = 1 - \Theta_f$ is defined as

$$\Theta_p = \frac{1}{V_{cv}} \sum_{k=1}^{N_p} V_{p,k} \mathcal{G}_\sigma \left(\vec{x}, \vec{x}_k\right) \tag{2}$$

where the summation is over all particles N_p. Here $\vec{x}_k$ is the particle location, $\vec{x}$ the centroid of a control volume, $V_{p,k}$ the volume of a particle, and V_{cv} the volume of the grid cell containing the particle centroid. The interpolation function effectively transfers Lagrangian quantity to give an Eulerian field on the underlying grid and is defined later. The fluid momentum equation is given as

$$\frac{\partial}{\partial t}\left(\rho_f \Theta_f \mathbf{u}_f\right) + \bigtriangledown \cdot \left(\rho_f \Theta_f \mathbf{u}_f \mathbf{u}_f\right) = - \bigtriangledown \left(\Theta_f p\right) + \bigtriangledown \cdot \left(\mu_f \mathbf{D}_c\right) + \mathbf{F} \tag{3}$$

where p is the average pressure, μ_f is the viscosity of the fluid, and $\mathbf{D}_c = \bigtriangledown \mathbf{u}_c + \bigtriangledown \mathbf{u}_c^T$ the average deformation-rate of the fluid-particle composite, $\mathbf{u}_c$ the composite velocity of the mixture [12], and F the force per unit volume exerted on the fluid by particles.

2.2 Dispersed-Phase Equations

The individual particle positions and velocities can be obtained by solving the ordinary differential equations in Lagrangian framework for each particle p :

$$\frac{d}{dt}(\mathbf{x}_p) = \mathbf{u}_p; \qquad m_p \frac{d}{dt}(\mathbf{u}_p) = F_p \tag{4}$$

where $\mathbf{x}_p$ is the particle position, $\mathbf{u}_p$ the particle velocity, $\mathbf{F}_p = m_p \mathbf{A}_p$ the total force acting on the particle of mass m_p, and $\mathbf{A}_p$ is the particle acceleration. This consists of the standard hydrodynamic drag force, dynamic pressure gradient, gradient of viscous stress in the fluid phase, a generalized buoyancy force, inter-particle collision and external body forces (gravity). In the present work, we assume that the particle forces consist of drag, collision and gravitational acceleration, and neglect all other terms in order to investigate the effect of the particle volume fraction. For high density ratios ($\rho_p/\rho_g \sim 1000$), these assumptions are valid [3]:

$$A_p = D_p(\mathbf{u}_f - \mathbf{u}_p) - \left(1 - \frac{\rho_f}{\rho_p}\right)\mathbf{g} + \mathbf{A}_{cp}. \tag{5}$$

Here $\mathbf{A}_{cp}$ is the acceleration due to inter-particle forces. The standard expression for drag force, D_p, is used

$$D_p = \frac{3}{8} C_d \frac{\rho_f}{\rho_p} \frac{|\mathbf{u}_f - \mathbf{u}_p|}{R_p}, \tag{6}$$

where C_d is the drag coefficient [13],

$$C_d = \frac{24}{Re}\left(1 + 0.15 Re_p^{0.687}\right)\Theta_f^{-2.65}, \quad for \quad Re_p < 1000 \tag{7}$$

$$= 0.44 \Theta_f^{-2.65}, \quad for \quad Re_p \geq 1000 \tag{8}$$

$R_p = (3V_p/4\pi)^{1/3}$ is the particle radius. The particle Reynolds number (Re_p) is given as, $Re_p = 2\rho_f \Theta_f |\mathbf{u}_f - \mathbf{u}_p| R_p/\mu_f$. There is an indirect collective effect in this drag term: when there is a dense collection of particles passing through the fluid, the interphase momentum exchange term in equation (3) will cause $\mathbf{u}_g$ to approach the particle velocity, $\mathbf{u}_p$, thus decreasing the drag on a particle, a drafting effect. The inter-particle collision scheme is based on the discrete element approach of Cundall & Strack as given in [9]. This is necessary to keep the particle centroids from overlapping each other. The interphase momentum transfer function per unit volume in equation (3) is given as

$$\mathbf{F} = \frac{1}{V_{cv}} \sum_{k=1}^{N_p} V_{p,k} \mathcal{G}_\sigma (\mathbf{u}_f - \mathbf{u}_p) \tag{9}$$

3 Numerical Method

In this work, we modify the numerical scheme for unstructured, arbitrary shaped elements developed by Mahesh *et al.* [14] to take into account the fluid volume fraction. On Cartesian grids in three-dimensions, bilinear interpolation functions utilizing 26 neighboring grid cells to interpolate Eulerian fields from the Lagrangian quantities have been used [8, 10]. In an effort to generalize these interpolations to unstructured, arbitrary shaped elements, we make use of a Gaussian distribution function centered at the particle centroid as an interpolation function and is given by,

$$\mathcal{G}_\sigma(\mathbf{x}, \mathbf{x}_p) = \frac{1}{\left(\sigma\sqrt{2\pi}\right)^3} exp\left[-\frac{\sum_{k=1}^{3} (x_k - x_{p,k})^2}{2\sigma^2} \right]. \tag{10}$$

Here we assume that $V_{p,k} < V_{cv}$ and set the filter width to be equal to the longest diagonal of the control volume (CV) containing the particle. The interpolation operator is applied to all the neighbors of the CV (having at least one grid node common). Similar interpolation function has been used in the context of resolved simulations of particles [15]. In addition, $\mathcal{G}$ is normalized to satisfy $\int_{V_{cv}} \mathcal{G}_\sigma \left(\mathbf{x} - \mathbf{x_{p,k}}\right) dV = 1$, where the integration is performed over all the neighbors of CV. The final step is necessary to enforce mass (or volume) conservation. The resulting Θ_p will be smooth and mass-conserving as the particles move from one CV to another. We use an implicit scheme for the fluid solver, however, the interphase momentum exchange terms are treated explicitly. The particle equations are integrated using third-order Runge-Kutta schemes for *ode*-solvers. At each Runge-Kutta step, the particles were relocated and the collision force was re-computed. We use the Lagrangian particle tracking algorithm developed in [3].

4 Results

4.1 Case 1: Gravitational Settling

We first simulate sedimentation of solid particles under gravity in a rectangular box. Details of this case are given in Table 1. The initial parcel positions are generated randomly over the box length. These particles are then allowed to settle through the gas-medium under gravity. The dominant forces on the particles include gravity and inter-particle/particle-wall collision. As the particles hit the bottom wall of the box, they bounce back and stop the incoming

Table 1. Parameter description for gravity-dominated sedimentation.

Computational domain, $0.2 \times 0.6 \times 0.0275m$	Grid, $10 \times 30 \times 5$
Fluid density, $1.254kg/m^3$	Particle Density, $2500kg/m^3$
Number of Parcels, 1000	Particles per parcel, 3375
Diameter of particles, $500\mu m$	Initial particle concentration, 0.2

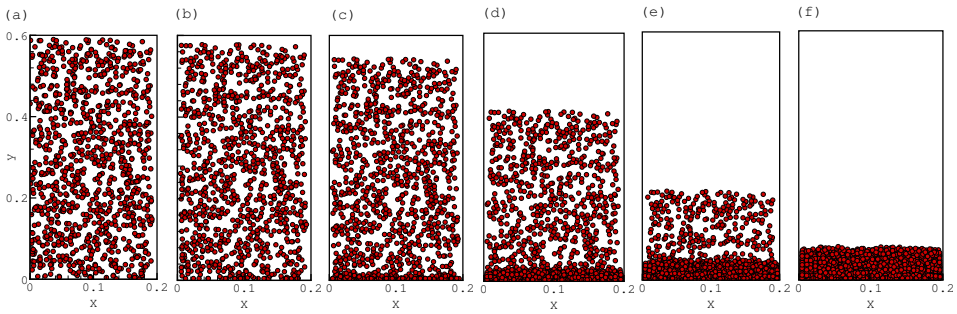

Fig. 1. Temporal evolution of particle distribution during gravity-dominated sedimentation.

layer of particles, and finally settle to a close pack limit. The upper mixture interface between the particles and the fluid is closely approximated by $h = gt^2/2$ [10]. As the particles settle the fluid in the bottom half of the box starts to move upward giving resistance to the settling particles. The evolution of the mixture interface closely follows the analytical estimate in our computation.

4.2 Case 2 : Fluidization by Jet

Table 2. Parameter description for the simulation of fluidization by a gas jet.

Computational domain, $0.2 \times 0.6 \times 0.0275m$	Grid, $10 \times 30 \times 5$
Gas jet velocity, $9m/s$	Jet diameter, $0.04m$
Fluid density, $1.254kg/m^3$	Particle Density, $2500kg/m^3$
Number of Parcels, 2880	Particles per parcel, 3375
Diameter of particles, $500\mu m$	Initial particle concentration, 0.4

We consider the problem of fluidization of solid particles arranged in an array at the bottom of a rectangular box. Fluidization is achieved by a jet of gas from the bottom of the box. The flow parameters are given in Table 2. The particle motion is mostly dominated by the hydrodynamic drag force

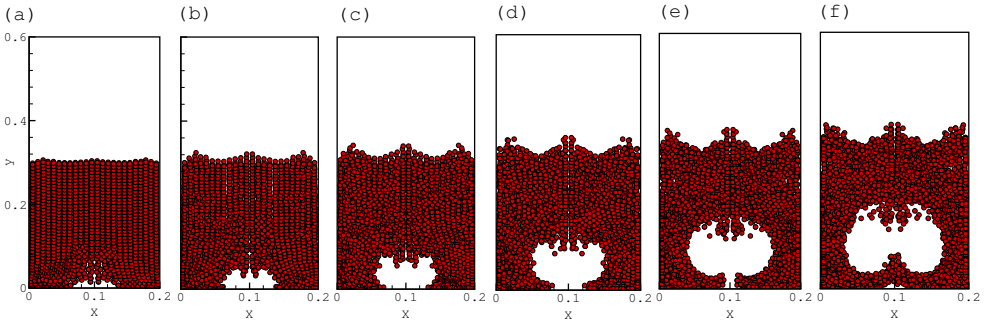

Fig. 2. Temporal evolution of particle distribution during fluidization by a gas jet. Initially all particles are uniformly arranged in layers at the bottom of the rectangular box. Air is injected through a rectangular slot at the bottom wall. Air bubbles are trapped within the particles and the growth and pattern of these bubbles are in agreement with simulations by Patankar & Joseph citePatankarJoseph01b.

and collision model should not affect the overall particle motion. The collision model, however, is important in governing the particle behavior near the walls and helps prevent the volume fraction from exceeding the close-pack limit.

Figure 2 shows the position of parcels at different times during bubbling fluidization. The jet issued from the bottom wall pushes the particles away from the center region and creates a gas-bubble in the center. The particles collide with each other, against the wall and are pushed back towards the central jet along the bottom wall. They are then entrained by the jet and are levitated. This eventually divides the central bubble to form two bubbles. The particles tend to move upward and collide with the upper wall and remain levitated during future times. The computational results are in good agreement with the simulations of [9]. Similar results are reported using Eulerian-Eulerian approach in two-dimensions [16].

4.3 Case 3: Fluidization by Lift

Table 3. Parameter description for the simulation of fluidization of spherical particles in a plane Poisuille flow.

Computational domain, $63 \times 12 \times 12 cm$	Grid, $20 \times 11 \times 10$
Fluid density, $1 g/cm^3$	Fluid viscosity, $1 poise$
Particle Density, $10.0 g/cm^3$	Diameter of particles, $0.95 cm$
Number of Parcels, 3780	Particles per parcel, 1
Initial array height, $4.75 cm$,	Initial centerline velocity, $360 cm/s$
Pressure gradient, $20 dyne/cm^3$	

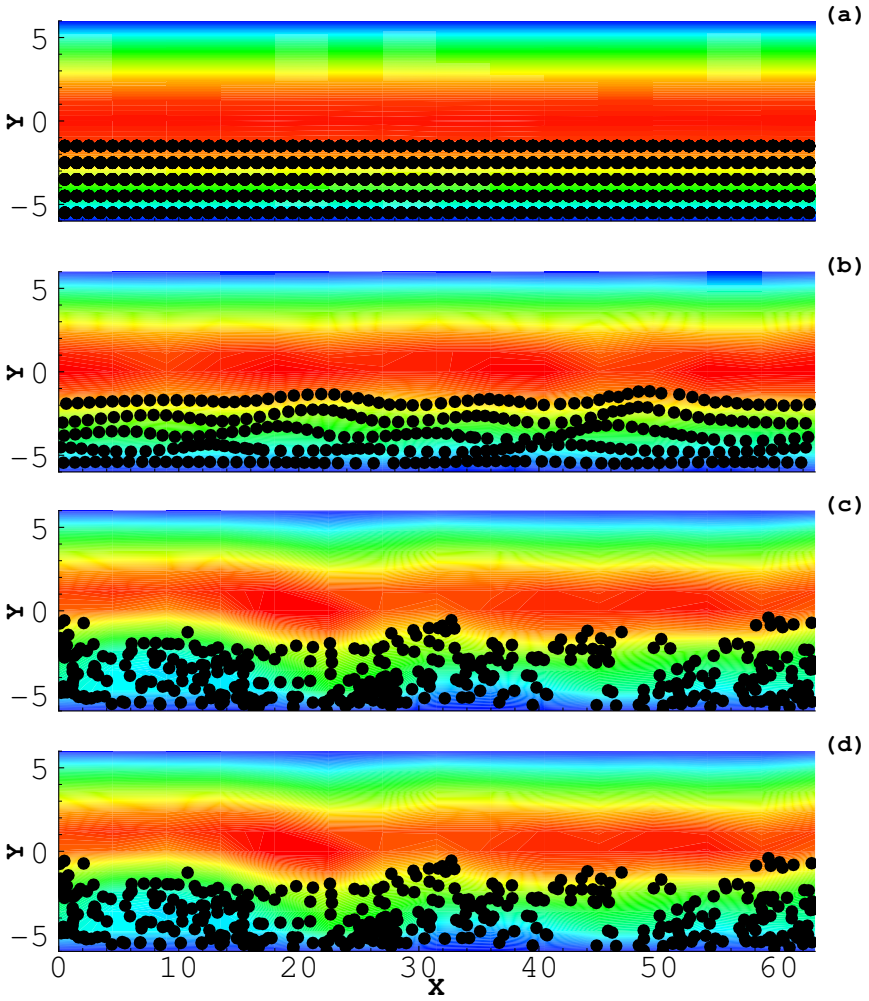

Fig. 3. Temporal evolution of axial velocity contours in a plane Poisuille flow with particles in the bottom half of the channel.

The transport of particles by fluids in coal-water slurries, hydraulically fractured rocks in oil-bearing reservoirs, bed-load transport in rivers and canals and their overall effect on the river bed erosion etc., are important scientific and industrial issues in particulate flows. In order to understand fluidization/sedimentation in such conduits, Choi & Joseph [1] performed a DNS study of fluidization of circular cylinders (300 particles) arranged at the bottom of a channel in plane Poisuille flow. They observed that with sufficient pressure gradient across the channel, the particles initially at rest in the lower

half of the channel start moving and roll over the wall. Particle rotation in a shear flow generates lift and the channel is fluidized after some time.

The flow parameters are given in Table 3. As opposed to [1], we are performing three-dimensional simulations. The particles initially at rest, accelerate and setup instability waves between the fluid and particle layers. Figure 3 shows the time-evolution of axial velocity contours in the fluid as well as particle locations in the $z = 0$ plane. As the fluid is pushed out of the control volume by motion of particles a vertical pressure gradient is created imparting vertical velocity to the particles and the channel gets fluidized. We also did several test cases, with higher grid resolution, increased density ratios to obtain similar results. With increased particle density, the inter-phase momentum exchange decelerates the fluid in the bottom half of a channel and an inflection point is created in the axial velocity profile. This eventually causes lift and particle dispersal. It should be noted that, the mechanism of lift observed in the DNS simulations is different from the one given by the model. In the model, we do not consider the changes in volume fraction due to particle rotation, however, the unsteady effects of particle motion are captured entirely through the particle volume fraction.

5 Discussion

We also simulated all the above cases using the point-particle approach with collisions [17]. For the first case (gravitational settling), the particle evolution obtained from point-particles and the finite-size model are similar. This is mainly because, the flow is gravity and collision dominated and there is no mean fluid flow. In the cases of fluidization, however, the particle evolutions are completely different. The patterns observed in figure 2 are absent when simulated using point-particles. Also, for the Poisuille flow, point-particles do not predict any lift and fluidization. This indicates that two-way coupling modeled using point-particles is not sufficient to produce the effects observed in direct numerical simulations of these flows. In the present formulation where we account for the volume displacement, the particle volume fraction alters the flow evolution in three-different ways: a) continuity equation, b) the momentum equation, and c) the drag force. The blocking effect of particles on the fluid phase, modeled by the continuity equation alters the fluid flow in regions of high gradients in volume fraction.

These findings have several implications on LES/DNS of two-phase flows. As mentioned earlier, the point-particle approach does not reproduce the turbulence attenuation obtained by solid particles in a channel flow even at moderate loadings compared to the experimental observations [4]. For such wall-bounded flows, the particles near the wall, tend to move slowly due to their inertia thus increasing their residence time near the wall. Inter-particle and particle-wall collisions play an important role. The grid resolution in the wall-normal direction is such that the particle diameter is typically occupied by

4-5 grid cells near the wall. In addition, due to increased residence times near the wall, the local particle volume fractions become high and gradients in the volume fraction field can alter the fluid flow. Prosperetti & Zhang [18] argued that the effect of volume fraction may be more important than inter-particle collisions in the near wall regions. As shown in the above case studies, considering the fluid displaced by the particles in the continuity and momentum equations has an indirect effect of increased particle loading on the fluid phase. Segura *et al.* [4] had to artificially increase the particle loading to match the experimental data on turbulence modulation. This suggests that the gradients in volume fraction field near the wall could account for these effects.

Furthermore, applications involving dense flows such as liquid-fuel atomization in automotive and aircraft engines, coal-fired combustion chambers, and fluidized beds, should account for the finite-size of the droplets/particles in order to predict the evolution of the fuel mass fractions correctly. As demonstrated by the last case above, instability waves created by dense fuel flowing in a lighter fluid can be captured by this model and will allow us to better represent the important features of primary atomization often neglected in these simulations [19].

6 Conclusions

In the present study we extend the point-particle approach typically employed in multiphase flows by accounting for the finite-size of the particles. The presence of particles affects the fluid phase continuity and momentum equations through the volume fraction field. Efficient interpolation scheme to obtain Eulerian fields from Lagrangian points on arbitrary shaped, unstructured meshes has been developed. The numerical technique has been applied to dense particulate flows such as gravitational settling and fluidization by a gaseous jet. Finally, we have shown that the present model can predict lift and fluidization of a plane channel flow with heavy particles arranged in layers at the bottom of the channel. These effects were captured entirely due to the fluid volume displaced by the particles and were not observed using the point-particle approach. Based on this study, we propose that for moderate loadings, the standard point-particle approach should be modified to account for the finite-size of the particles. Further investigations on turbulent flows at moderate to high particle loadings are necessary.

7 Acknowledgement

Support for this work was provided by the United States Department of Energy under the Accelerated Strategic Computing (ASC) program.

References

1. Choi, H.G., & Joesph, D.D. (2001) J. Fluid. Mech. 438:101–128.
2. Patankar, N. A., Ko, T., Choi, H. G. & Joseph, D. D. (2001) J. Fluid Mech. 445:55–76.
3. Apte, S. V., Mahesh, K., Moin, P., & Oefelein, J.C. (2003a) Int. J. Mult. Flow 29:1311–1331.
4. Segura, J. C., Eaton, J. K. & Oefelein, J. C. (2004) Predictive capabilities of particle-laden LES. Rep. No. TSD–156, Dept. of Mech. Engng., Stanford University.
5. Burton, T. M. & Eaton, J. K. (2003) Fully resolved simulations of particle-turbulence interaction. Rep. No. TSD–151, Dept. of Mech. Engng., Stanford University.
6. Bagchi, P. & Balachandar, S. (2003) Phys. Fluids 15:3496–3513.
7. Dukowicz, J. K. (1980) J. Comput. Phys. 35:229–253.
8. Patankar, N. A., & Joseph, D. D. (2001a) Int. J. Multi. Flow 27:1659–1684.
9. Patankar, N. A., & Joseph, D. D.(2001b) Int. J. Multi. Flow 27:1685–1706.
10. Snider, D. M. (2001) J. Comput. Phys. 170:523–549.
11. Ferrante, A., & Elghobashi, S. (2004) J. Fluid Mech. 503:345–355
12. Joseph, D.D., & Lundgren, T. (1990) Int. J. Mult. Flow 6:35–42.
13. Andrews, M. J., & O'Rourke, P. 1996 Int. J. Mult. Flow 22:379–402.
14. Mahesh, K., Constantinescu, G.,& Moin, P. (2004). J. Comput. Phys. 197(1):215–240.
15. Maxey, M.R., & Patel, B.K. (2001) Int. J. Mult. Flow. 27:1603–1626.
16. Ding, J. & Gidaspow, D. (1990) AIChE 36:523–537.
17. Apte, S.V., Mahesh, K., & Lundgren, T. (2005) J. Fluid Mech. *to be submitted.*
18. Prosperetti, A., & Zhang, D.Z. (1995) Theo. Comp. Fluid. Dyn. 7:429–440.
19. Moin, P., & Apte, S.V. (2004) Large-eddy simulation of realistic gas-turbine combustors AIAA Paper: 2004-0330, Reno, NV.